Letter

Topological piezoelectric response in moiré graphene systems

Ran Peng
School of Physical Science and Technology, ShanghaiTech University, Shanghai 201210, China

Jianpeng Liu*
School of Physical Science and Technology, ShanghaiTech University, Shanghai 201210, China
and ShanghaiTech Laboratory for Topological Physics, ShanghaiTech University, Shanghai 201210, China

(Received 26 September 2021; accepted 25 May 2022; published 11 July 2022)

We theoretically study the piezoelectric effects in moirè graphene systems. Since the strain couples to the electrons in the system as an effective vector field, which has opposite signs for the K and K' valleys of graphene, its effects on the two valleys with opposite Chern numbers do not cancel out, but adds up. As a result, some components of the piezoelectric tensor (PET) in these systems, which typically have nontrivial topology in their flat bands, are nearly quantized in terms of the valley Chern numbers. The quantization of the PET is topologically protected by valley $U(1)$ symmetry of the system. Such a conclusion is verified by numerical calculations of the in-plane piezoelectric response of hBN-aligned twisted bilayer graphene (TBG), twisted bilayer-monolayer graphene (TBMG), and twisted double bilayer graphene (TDBG) systems using both continuum model and atomistic tight-binding model. We propose that such nearly quantized piezoelectric response may serve as a direct experimental probe for the valley Chern numbers of the flat bands in moiré graphene systems.

DOI: 10.1103/PhysRevResearch.4.L032006

The intriguing phenomena, such as superconductivity [1–8], correlated insulating states [4–7,9–14], and quantum anomalous Hall states [14–16], observed in TBG around magic angle, has drawn great attention in recent years. This attention soon extends to twisted multilayer graphene systems such as twisted bilayer-monolayer graphene [17–19] and twisted double bilayer graphene systems [20–23], and to hBN-graphene heterostructures [24,25], which exhibit equally interesting properties. All these exotic effects are believed to be attributed by the low-energy flat bands in these moiré graphene systems, which are found to be topologically nontrivial [26–32].

In magic-angle TBG, the low-energy states can be divided into two sets: one from the K valley, and the other from the K' valley of graphene, each of which covers the entire moiré Brillouin zone [33,34]. Moreover, by virtue of the large moiré superlattice constant $L_s \sim 10\,\text{nm}$, the intervalley scattering induced by the long-period moiré potential between the two sets of low-energy states is negligible [33,34], thus the total charge of each valley is separately conserved characterized by valley $U(1)$ symmetry [35]. This means that one can separately define topological quantities, such as Wilson loops [27,29,36] and opposite Chern numbers [28,31,32] for the two valleys, known as valley Chern numbers (VCNs). However, direct evidence of the nontrivial VCNs of the moiré graphene systems from experiments are still absent. On one hand, the expected gapless helical topological edge states would be gapped out by the significantly enhanced intervalley scatterings due to the atomic-scale potentials from the sample boundaries. On the other hand, without interaction-driven spontaneous valley polarization, the topological effects from the nonzero VCNs always cancel each other due to time-reversal (TR) symmetry, which cannot be separated by tuning the carrier density. This is true for most measures of tuning the materials, with one possible exception—strain. In low-energy bands, strain does not act on the two valleys in equal way, but oppositely. A valley dependent effective vector field can be induced by strain, which is opposite in the two valleys associated by TR operation. As a result, strain effect on opposite valleys does not cancel each other, but adds up.

The above reasoning applies to generic twisted multilayer graphene (TMG) and other moiré graphene heterostructure systems, which typically have topological flat bands with nonzero VCNs that are highly tunable by displacement fields and twist angle [31,32,37–39]. Such nontrivial topological properties motivate us to study the strain effects in this whole series of systems. In the continuum model framework, we argue that the piezoelectric response of these twisted graphene systems are (nearly) quantized, in the sense that they can be expressed as a constant multiplied by the valley Chern numbers of the system. Taking hBN-aligned TBG, TBMG, and TDBG as examples, we have numerically calculated the piezoelectric response based on both continuum model and atomistic tight-binding models, and nearly quantized

*liujp@shanghaitech.edu.cn

Published by the American Physical Society under the terms of the Creative Commons Attribution 4.0 International license. Further distribution of this work must maintain attribution to the author(s) and the published article's title, journal citation, and DOI.

plateaus of piezoelectric tensors are obtained in all of the three systems.

a. Theories of polarization and piezoelectric response — According to the modern theory of polarization [40,41], polarization in an insulating crystal is measured by the charge current in an adiabatic evolution that establishes the final polarized state. The theory suggests a Berry-phase-like expression for the dependence of the polarization vector $\mathbf{P}$ on the adiabatic parameter λ [40,41]

$$\frac{\partial \mathbf{P}}{\partial \lambda} = \frac{e}{(2\pi)^2} \int d^2\mathbf{k} \sum_n \Omega_{\mathbf{k}\lambda,n}, \tag{1}$$

where $\Omega_{\mathbf{k}\lambda,n} = i(\langle \nabla_{\mathbf{k}} u_{n\mathbf{k}} | \partial_\lambda u_{n\mathbf{k}} \rangle - \langle \partial_\lambda u_{n\mathbf{k}} | \nabla_{\mathbf{k}} u_{n\mathbf{k}} \rangle)$, and $|u_{n\mathbf{k}}\rangle$ refers to the periodic part of the nth occupied Bloch function of the system. Note that Eq. (1) is correct even for a band with nonzero Chern number, although there is subtlety in considering the filling of edge states of a Chern insulator in the adiabatic process [42].

On the other hand, the Chern number of an isolated band $|u_{n\mathbf{k}}\rangle$ of a 2D crystal is expressed as

$$C_n = \frac{1}{2\pi i} \int d^2\mathbf{k} (\langle \partial_{k_x} u_{n\mathbf{k}} | \partial_{k_y} u_{n\mathbf{k}} \rangle - \langle \partial_{k_y} u_{n\mathbf{k}} | \partial_{k_x} u_{n\mathbf{k}} \rangle). \tag{2}$$

The similarity between Eq. (2) and Eq. (1) indicates a possibility of topological effects to show up in 2D crystal polarization. Since strain couples to electrons as an effective vector field, and the coupling coefficients have opposite signs for the opposite valleys (K and K'), we conjecture that the strain induced polarization, i.e., the piezoelectric response, may be the correct quantity to manifest nonzero VCNs of the moiré graphene systems.

The piezoelectric response is normally known as the change of polarization $\mathbf{P}$ induced by the strain tensor μ_{jk}: $\gamma_{ijk} = \partial P_i / \partial \mu_{jk}$, which turns out to be "improper" due to possible ambiguities [43]. A proper definition of piezoelectric response tensor is expressed as [43] $\gamma_{ijk} = \partial \dot{P}_i / \partial \dot{\mu}_{jk}$, where $\dot{P}_i$ and $\dot{\mu}_{jk}$ denote the time derivatives of the polarization and the strain, with $i, j, k = x, y$ for 2D systems. The strain tensor is defined by the shift $\Delta\mathbf{r}$ of a real-space position $\mathbf{r}$ with respect to the original position $\mathbf{r}$: $\Delta r_i = \sum_{j,k=x,y} \mu_{ij} r_j$. By simply replacing the adiabatic parameter λ in Eq. (1) with strain component μ_{jk}, and multiplying both sides of Eq. (1) by $\dot{\mu}_{jk}$, we obtain the expression for the PET component contributed from the valley η ($\eta = \pm$ refers to the K and K' valleys) in the twisted graphene system:

$$\gamma^\eta_{ijk} = \frac{e}{(2\pi)^2} \int d^2\mathbf{k}\, \Omega^\eta_{ijk}, \tag{3}$$

where

$$\Omega^\eta_{ijk} = \sum_n i(\langle \partial_{k_i} u_{\eta,n\mathbf{k}} | \partial_{\mu_{jk}} u_{\eta,n\mathbf{k}} \rangle - \langle \partial_{\mu_{jk}} u_{\eta,n\mathbf{k}} | \partial_{k_i} u_{\eta,n\mathbf{k}} \rangle). \tag{4}$$

Here the index n refers to the occupied band of the η valley. A small homogeneous strain applied to the system is equivalent to an effective vector field $A^\eta_i = \xi^\eta_{ijk} \mu_{jk}$ in the η valley [44–48], which is linearly coupled to the wavevector: $\mathbf{k} \to \mathbf{k} + \mathbf{A}^\eta$, and the partial derivative with respect to strain in Eq. (4) can be substituted by a partial derivative with respect to wavevector: $\partial_{\mu_{jk}} = \xi^\eta_{ijk} \partial_{k_i}$. As will be discussed in detail below, the prefactor ξ^η_{ijk} only depends on the properties of monolayer graphene, and is of opposite sign for the opposite valleys. Therefore, the opposite Chern numbers together with opposite strain effects means that the PET contributed by the two valleys should be the same, and is exactly quantized in terms of the VCNs of the occupied bands multiplied by a constant:

$$\gamma_{ijk} = 2(-1)^i \frac{e}{2\pi} (\xi^-_{ijk} C_- + \xi^+_{ijk} C_+), \tag{5}$$

where $C_\pm$ is the Chern number of the occupied bands from the K and K' valleys, and $(-1)^i = \pm 1$ for $i = x, y$. The prefactor 2 accounts for the spin degeneracy. The quantization of the PET can be intuitively interpreted as follows. Let us consider the situation that the strain-induced effective vector field $\mathbf{A}^\eta$ is adiabatically turned on in the system, which imposes opposite effective "electric fields" $\mathbf{E}^\eta = -\dot{\mathbf{A}}^\eta$ ($\eta = \pm$) to the two valleys, which in turn induce transverse adiabatic "Hall currents" from the two valleys with opposite Chern numbers. The "Hall currents" generated from the two valleys are the same since both the Chern numbers and the effective electric fields are opposite. The piezoelectric tensor, e.g., γ_{yxx}, measures precisely the "Hall conductivity" of the adiabatic current in the process of adiabatically turning on the strain, and such response is naturally quantized in units of VCNs of the system. In a previous paper [49], it is shown that for topologically nontrivial 2D crystalline materials with TR symmetry, a jump of piezoelectric response is expected near a topological phase transition (TPT). In the above argument, we show that in moiré graphene systems the PET does not only exhibit discontinuity across a TPT, but are always quantized in units of the VCNs of the occupied bands no matter the system is close to a TPT or not. This is a unique property for the topologically nontrivial bands with nonzero VCNs in moiré graphene systems, which is topologically protected by valley $U(1)$ symmetry.

b. Model Hamiltonian — To illustrate the idea of quantized PET, we first study the PET of hBN-aligned TBG based on Bistritzer-MacDonald continuum Hamiltonian [33,50,51]. The effects of the hBN alignment is modelled by imposing a staggered sublattice potential $\Delta = 15$ meV to both layers, neglecting the moiré potential introduced by the lattice match between hBN and graphene [28,31,52,53]. The aligned hBN substrate breaks C_{2z} symmetry, opening a gap ~ 4 meV between the conduction and valence bands [see Fig. 1(b)], which have nonzero VCNs ± 1. The original D_6 symmetry of the continuum model is reduced to D_3 symmetry, which requires the PET components subject to the following relation: $\gamma_{xxx} = \gamma_{xyy} = \gamma_{yxy} = 0$, $\gamma_{xxy} = \gamma_{yxx} = -\gamma_{yyy}$. As a result of the threefold rotational symmetry, there is only one independent PET component γ_{yxx}. Therefore we choose to illustrate our results through the component γ_{yxx} for all twisted graphene systems discussed in this paper.

The Hamiltonian in the continuum model of TBG in K_η ($\eta = \pm$ represents K and K' valleys, respectively) is expressed as

$$H^\eta(\mathbf{r}) = \begin{pmatrix} H^\eta_1 & U_{\mathrm{M}}(\mathbf{r}) \\ U^\dagger_{\mathrm{M}}(\mathbf{r}) & H^\eta_2 \end{pmatrix}, \tag{6}$$

where the diagonal blocks H^η_l are the monolayer layer graphene (MLG) Dirac cones at K_η valley of layer l. The

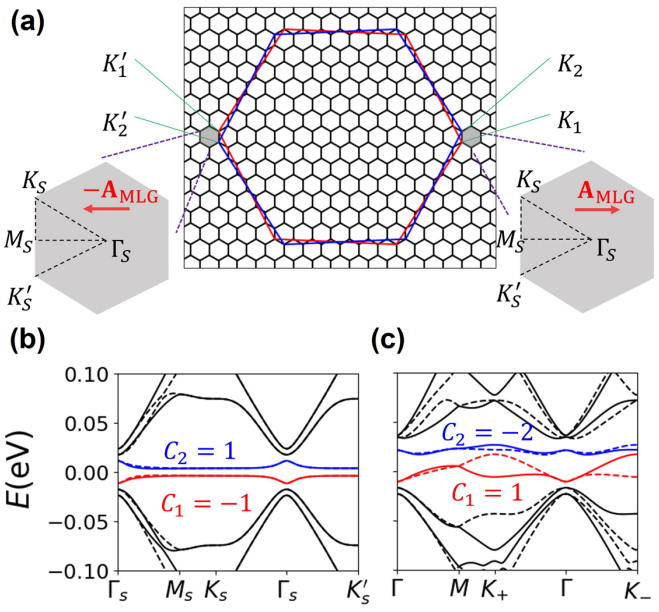


FIG. 1. (a) A plot of the Brillouin zones of the two layers of monolayer graphene (MLG) and the moirè Brillouin zone (mBZ) of TBG. The insets zoom in the moirè Brillouin zones near the $K(K')$ valleys with the high symmetry path being marked, and the opposite strain induced vector fields are schematically marked. [(b),(c)] The band structures of: (b) TBG with staggered sublattice potential $\Delta = 15\,\mathrm{meV}$ at $\theta = 1.05°$, (c) twisted bilayer-monolayer graphene with vertical electrostatic potential energy difference $U_d = -0.0536\,\mathrm{eV}$ (see text) at $\theta = 1.2°$.

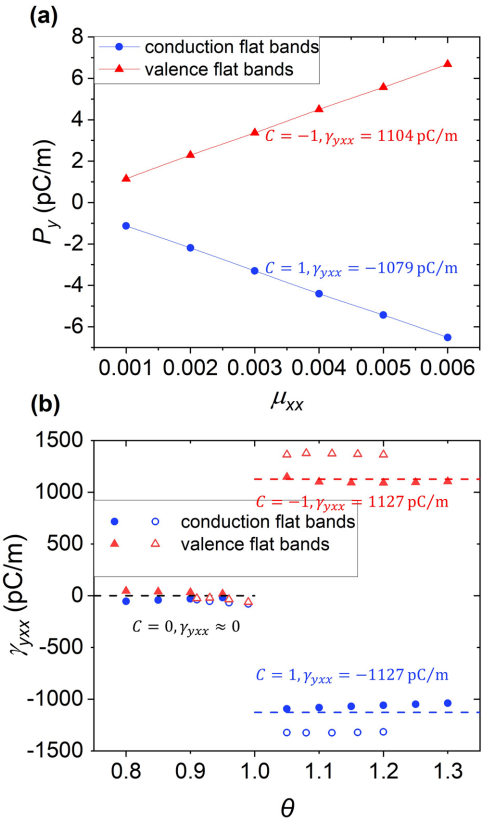


FIG. 2. (a) Plots of polarization along y direction vs strain u_{xx} for hBN-aligned TBG at $\theta = 1.05°$, and (b) twist-angle (θ) dependence of γ_{yxx} contributed by the valence (red triangles) and conduction (blue circles) flat bands, where the solid ones are the results from continuum model and the hollow ones are the results from tight-binding model. The horizontal-dashed lines in (b) mark the ideal quantized values.

off-diagonal block, which represents the interlayer coupling between the twisted bilayers introduces a moiré potential in real space $U_M(\mathbf{r})$ (see Supplemental Material [54]). As mentioned in the previous section, a homogeneous strain applied to the system is equivalent to a pseudo vector potential [44,45,55–58]. Here we ignore the effects of strain on the interlayer hopping [47], which are considered as higher-order effects, then the strain effects are only manifested in the diagonal blocks, which become [45,46,48]

$$H_l^\eta = \hbar v_F\,(\mathbf{q} + \eta \mathbf{A}_{\mathrm{MLG}}) \cdot (\eta\sigma_x, \sigma_y) + \Delta\sigma_z, \tag{7}$$

where $\mathbf{q} = \mathbf{k} - \mathbf{K}_{l,\eta}$. For MLG in its K valley,

$$\mathbf{A}_{\mathrm{MLG}} = -\frac{\sqrt{3}\beta}{2a}(\mu_{xx} - \mu_{yy}, -2\mu_{xy}), \tag{8}$$

where $a = 2.46$ Å is the lattice constant of MLG and $\beta = 3.14$ is the decaying rate of the hopping amplitude with respect to the distance between two carbon atoms in MLG [47,59]. This expression of strain induced vector field together with Eq. (5) tells us that in TBG system, the PET component γ_{yxx} per spin per VCN is

$$\gamma_{yxx}^0 = \frac{e}{2\pi}\frac{\sqrt{3}\beta}{2a} = -281.8\ \mathrm{pC/m}. \tag{9}$$

Note that γ_{yxx}^0 only depends on two parameters: the graphene lattice constant a and the hopping decaying rate β, both of which are "fundamental constants" in the universe of graphene-based systems. In a more realistic situation, the value of β can be modified due to interaction effects, and can be extracted from experimentally measured deformation potential ΔW via the relationship $\Delta W = 3\sqrt{3}\beta t_1(\mu_{xx} + \mu_{yy})/2$ with t_1 being the second-neighbor hopping amplitude in graphene. From Ref. [60], it follows that the experimentally measured deformation potential $\Delta W \approx 0.161$ eV under a 7% uniaxial strain, and correspondingly $\beta \approx 3.9$, leading to a modified quantization unit $\gamma_{yxx}^0 \approx -350$ pC/m. However, the fact that the PET is quantized in units of γ_{yxx}^0 remains robust.

In Fig. 2(a) we present the polarization along y direction as a function of strain u_{xx}, with twist angle $\theta = 1.05°$ for hBN-aligned TBG, where the blue circles and red triangles represent the contributions from the valence and conduction flat bands with opposite Chern numbers ± 1. Clearly the strain-induced polarizations are opposite from the two flat bands, indicating opposite PETs. In Fig. 2(b) we show the PET γ_{yxx} contributed by the valence (blue circles) and conduction (red triangles) flat bands as a function of twist angle θ. When $\theta \gtrapprox 1°$, the VCNs of the two flat bands are ± 1, the calculated γ_{yxx} is around the expected quantization value $\pm 4\gamma_{yxx}^0$ (marked by the dashed lines), where the prefactor 4 is from the fourfold valley-spin degeneracy. Under the present parameter choice, when $\theta \lessapprox 1°$, there is a TPT due to gap closures between the flat bands and the remote bands, such that the VCNs of the flat bands become zeros. As a result,

γ_{yxx} rapidly drops and becomes negligibly small as shown in Fig. 2(b). The plateau shape of γ_{yxx}-θ relationship supports our argument for the quantized PET. Since the quantized piezoelectric response is topologically protected by valley $U(1)$ symmetry, it remains robust against perturbations such as long-wavelength inhomogeneous strain [61] and interlayer optical strain (heterostrain) [10,61], which preserve valley $U(1)$ symmetry. However, at certain partial integer fillings of the flat bands, the ground states of TBG may spontaneously break valley $U(1)$ symmetry, forming intervalley coherent states [62–67]. In such a situation, the quantization of γ_{yxx} is no longer protected (see Supplemental Material [54]).

c. PET in TMG systems — The continuum model for TBG can be readily extended to TMG systems, for valley η, the Hamiltonian is expressed as [32]

$$H^{\eta}_{M,\alpha;N,\alpha'} = \begin{pmatrix} H^{\eta}_{M,\alpha} & U \\ U^{\dagger} & H^{\eta}_{N,\alpha'} \end{pmatrix}, \tag{10}$$

where we refer readers to Supplemental Material [54] for more details. The band structures for TBMG calculated using the continuum model is presented in Fig. 1(c) with Chern numbers of the flat bands from the K valley being marked. It is worthwhile to note that, with a realistic description of the system including further neighbor interlayer hoppings within each set of the untwisted multilayers [54], the strain may couple to the interlayer hopping in a similar, but slightly different way from how it couples to the intralayer hopping terms. The effective vector field associated with further-neighbor interlayer hopping event is expressed as

$$\mathbf{A}_{\text{inter}} = -\lambda\frac{\sqrt{3}\beta}{2a}(\mu_{xx} - \mu_{yy}, 2\mu_{xy}) = \lambda\mathbf{A}_{\text{MLG}}, \tag{11}$$

where $\lambda = a_0/\sqrt{a_0^2 + d_{\text{AB}}^2}$, with $a_0 = a/\sqrt{3} \approx 1.42$ Å and $d_{\text{AB}} = 3.35$ Å being the in-plane carbon-carbon σ-bond length and the interlayer distance between AB-stacked bilayer graphene respectively. As a result of the different strain-momentum coupling terms, the substitution $\partial_{\mu_{jk}} = \xi_{ijk}\partial_{k_i}$ in deriving Eq. (5) no longer holds. Luckily, since this quantization-breaking mechanism only occurs in the further-neighbor interlayer hopping terms (see Supplemental Material [54]), for typical TMGs such as TBMG, and TDBG systems, the deviations of PET from the ideal quantizated values are very weak (see Fig. 3).

In Fig. 3, we show γ_{yxx} component as a function of twist angle θ and vertical potential energy drop across the multilayers, denoted by U_d. As suggested by Ref. [32], in the chiral limit, the total VCNs of the two flat bands per spin equals to ± 1 for TBMG and ± 2 for AB-BA stacked TDBG. This conclusion conforms to the calculated values of γ_{yxx} and VCNs in the largest plateau of each subplot of Fig. 3. As the further neighbor interlayer hoppings and external displacement fields break the chiral limit, the total VCNs of the two flat bands change as a function U_d and θ, as shown in Figs. 3(c) and 3(d) for TBMG and TDBG, respectively, hence making the PETs jump to different quantized plateaus as shown in Figs. 3(a) and 3(b). The calculated PETs and VCNs agree with each other very well. As the flat bands are isolated from the remote bands for these TMG systems [17,18,20–23,68], the PET contributed by

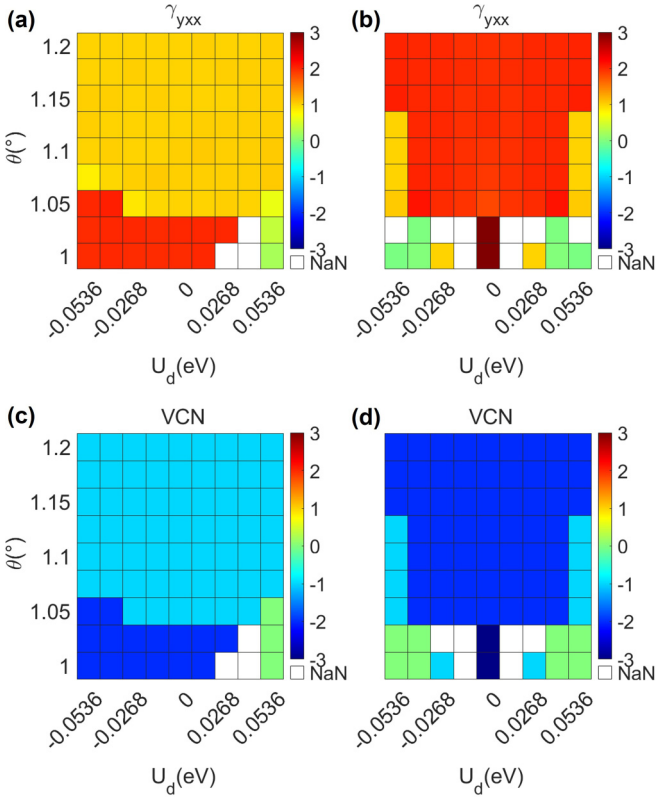


FIG. 3. PET and VCNs of all flat bands in TBMG and TDBG systems: (a) γ_{yxx} of TBMG as a function of θ and U_d; (b) γ_{yxx} of AB-BA stacked TDBG as a function of θ and U_d; (c) Total Chern numbers of the two flat bands from K valley of TBMG as a function of θ and U_d; (d) Total Chern numbers of the two flat bands from K valley of AB-BA stacked TDBG as a function of θ and U_d. In (a) and (b), the values of γ_{yxx} are shown in the units of $|4\gamma^0_{yxx}| = 1127$ pC/m. The blank patches indicate points, which are too close to gap closures such that VCNs are ill defined.

the flat bands can be extracted by comparing the PETs when the flat bands are fully occupied and empty.

The above argument of quantized PET is based on two approximations: (i) the K and K' valleys are decoupled, which is an excellent approximation and is widely adopted in literatures, and (ii) the effects of strain on the moiré potentials have been neglected, which deserves further verification. We have further checked the validity of approximation (ii) by directly calculating the piezoelectric response of hBN-aligned TBG and TBMG based on a realistic atomistic tight-binding model adopted from Ref. [59], which can include all the strain effects on the electronic structures. For hBN-aligned TBG, as shown in Fig. 2(b), our results indicate that γ_{yxx} *vs.* θ plot still exhibits a plateau shape with an abrupt jump at $\theta \approx 1^\circ$ due to a TPT (VCNs become zeros for $\theta \lessapprox 1^\circ$) although the quantization is not quite exact due to the strain effects on the moiré potential, with $\gamma_{yxx} \approx \pm 1.2 \times 4\gamma^0_{yxx}$ when the VCNs are ± 1. We have also calculated the U_d dependence of γ_{yxx} in TBMG contributed by the two flat bands at $\theta = 1.25^\circ$, and find a plateau of $\gamma_{yxx} \approx 1.15 \times 4\gamma^0_{yxx}$ (see Supplemental Material [54]), compatible with the total VCN ± 1.

In this paper we apply the modern polarization theory to the case of piezoelectric response in moirè graphene sys-

tems, and find that certain components of the piezoelectric response tensor is quantized in units of VCNs, which is protected by valley $U(1)$ symmetry in the system. We suggest that the in-plane piezoelectric response can be measured based on a revised version of the piezoelectric force microscopy. Instead of applying a vertical AC voltage, one can apply a lateral voltage to the moiré system, then measure the in-plane lattice deformations induced by the electric field through the lateral deflections of the cantilever [69], from which the in-plane piezoelectric coefficient may be quantitatively determined. Our paper thus suggests a plausible and feasible way of measuring the VCNs in these systems based on quantized piezoelectric coefficient, which will provide useful guidelines for further experimental and theoretical studies.

This work is supported by the National Key R & D program of China (Grant No. 2020YFA0309601), the National Natural Science Foundation of China (Grant No. 12174257), and the Start-up Grant of ShanghaiTech University. We would like to thank Jiamin Xue, Yue Zhao, Bin Cheng, and Moyu Chen for valuable discussions.

[1] Y. Cao, V. Fatemi, S. Fang, K. Watanabe, T. Taniguchi, E. Kaxiras, and P. Jarillo-Herrero, Unconventional superconductivity in magic-angle graphene superlattices, Nature (London) **556**, 43 (2018).

[2] M. Yankowitz, S. Chen, H. Polshyn, Y. Zhang, K. Watanabe, T. Taniguchi, D. Graf, A. F. Young, and C. R. Dean, Tuning superconductivity in twisted bilayer graphene, Science **363**, 1059 (2019).

[3] E. Codecido, Q. Wang, R. Koester, S. Che, H. Tian, R. Lv, S. Tran, K. Watanabe, T. Taniguchi, F. Zhang *et al.*, Correlated insulating and superconducting states in twisted bilayer graphene below the magic angle, Sci. Adv. **5**, eaaw9770 (2019).

[4] X. Lu, P. Stepanov, W. Yang, M. Xie, M. A. Aamir, I. Das, C. Urgell, K. Watanabe, T. Taniguchi, G. Zhang *et al.*, Superconductors, orbital magnets and correlated states in magic-angle bilayer graphene, Nature (London) **574**, 653 (2019).

[5] P. Stepanov, I. Das, X. Lu, A. Fahimniya, K. Watanabe, T. Taniguchi, F. H. L. Koppens, J. Lischner, L. Levitov, and D. K. Efetov, Untying the insulating and superconducting orders in magic-angle graphene, Nature (London) **583**, 375 (2020).

[6] Y. Saito, J. Ge, K. Watanabe, T. Taniguchi, and A. F. Young, Independent superconductors and correlated insulators in twisted bilayer graphene, Nat. Phys. **16**, 926 (2020).

[7] X. Liu, Z. Wang, K. Watanabe, T. Taniguchi, O. Vafek, and J. Li, Tuning electron correlation in magic-angle twisted bilayer graphene using coulomb screening, Science **371**, 1261 (2021).

[8] Y. Cao, D. Rodan-Legrain, J. M. Park, N. F. Yuan, K. Watanabe, T. Taniguchi, R. M. Fernandes, L. Fu, and P. Jarillo-Herrero, Nematicity and competing orders in superconducting magic-angle graphene, Science **372**, 264 (2021).

[9] Y. Cao, V. Fatemi, A. Demir, S. Fang, S. L. Tomarken, J. Y. Luo, J. D. Sanchez-Yamagishi, K. Watanabe, T. Taniguchi, E. Kaxiras *et al.*, Correlated insulator behaviour at half-filling in magic-angle graphene superlattices, Nature (London) **556**, 80 (2018).

[10] A. Kerelsky, L. J. McGilly, D. M. Kennes, L. Xian, M. Yankowitz, S. Chen, K. Watanabe, T. Taniguchi, J. Hone, C. Dean *et al.*, Maximized electron interactions at the magic angle in twisted bilayer graphene, Nature (London) **572**, 95 (2019).

[11] Y. Jiang, X. Lai, K. Watanabe, T. Taniguchi, K. Haule, J. Mao, and E. Y. Andrei, Charge order and broken rotational symmetry in magic-angle twisted bilayer graphene, Nature (London) **573**, 91 (2019).

[12] Y. Xie, B. Lian, B. Jäck, X. Liu, C.-L. Chiu, K. Watanabe, T. Taniguchi, B. A. Bernevig, and A. Yazdani, Spectroscopic signatures of many-body correlations in magic-angle twisted bilayer graphene, Nature (London) **572**, 101 (2019).

[13] Y. Choi, J. Kemmer, Y. Peng, A. Thomson, H. Arora, R. Polski, Y. Zhang, H. Ren, J. Alicea, G. Refael *et al.*, Electronic correlations in twisted bilayer graphene near the magic angle, Nat. Phys. **15**, 1174 (2019).

[14] M. Serlin, C. Tschirhart, H. Polshyn, Y. Zhang, J. Zhu, K. Watanabe, T. Taniguchi, L. Balents, and A. Young, Intrinsic quantized anomalous hall effect in a moiré heterostructure, Science **367**, 900 (2019).

[15] A. L. Sharpe, E. J. Fox, A. W. Barnard, J. Finney, K. Watanabe, T. Taniguchi, M. A. Kastner, and D. Goldhaber-Gordon, Emergent ferromagnetism near three-quarters filling in twisted bilayer graphene, Science **365**, 605 (2019).

[16] P. Stepanov, M. Xie, T. Taniguchi, K. Watanabe, X. Lu, A. H. MacDonald, B. A. Bernevig, and D. K. Efetov, Competing Zero-Field Chern Insulators in Superconducting Twisted Bilayer Graphene, Phys. Rev. Lett. **127**, 197701 (2020).

[17] H. Polshyn, J. Zhu, M. Kumar, Y. Zhang, F. Yang, C. Tschirhart, M. Serlin, K. Watanabe, T. Taniguchi, A. MacDonald *et al.*, Electrical switching of magnetic order in an orbital chern insulator, Nature (London) **588**, 66 (2020).

[18] S. Chen, M. He, Y.-H. Zhang, V. Hsieh, Z. Fei, K. Watanabe, T. Taniguchi, D. H. Cobden, X. Xu, C. R. Dean, and M. Yankowitz, Electrically tunable correlated and topological states in twisted monolayer–bilayer graphene, Nat. Phys. **17**, 374 (2021).

[19] S. Xu, M. M. Al Ezzi, N. Balakrishnan, A. Garcia-Ruiz, B. Tsim, C. Mullan, J. Barrier, N. Xin, B. A. Piot, T. Taniguchi *et al.*, Tunable van Hove singularities and correlated states in twisted monolayer–bilayer graphene, Nat. Phys. **17**, 619 (2021).

[20] X. Liu, Z. Hao, E. Khalaf, J. Y. Lee, Y. Ronen, H. Yoo, D. Haei Najafabadi, K. Watanabe, T. Taniguchi, A. Vishwanath, and P. Kim, Tunable spin-polarized correlated states in twisted double bilayer graphene, Nature (London) **583**, 221 (2020).

[21] C. Shen, Y. Chu, Q. Wu, N. Li, S. Wang, Y. Zhao, J. Tang, J. Liu, J. Tian, K. Watanabe, T. Taniguchi, R. Yang, Z. Y. Meng, D. Shi, O. V. Yazyev, and G. Zhang, Correlated states in twisted double bilayer graphene, Nat. Phys. **16**, 520 (2020).

[22] Y. Cao, D. Rodan-Legrain, O. Rubies-Bigorda, J. M. Park, K. Watanabe, T. Taniguchi, and P. Jarillo-Herrero, Tunable correlated states and spin-polarized phases in twisted bilayer–bilayer graphene, Nature (London) **583**, 215 (2020).

[23] C. Rubio-Verdú, S. Turkel, L. Song, L. Klebl, R. Samajdar, M. S. Scheurer, J. W. F. Venderbos, K. Watanabe, T. Taniguchi,

H. Ochoa *et al.*, Universal moiré nematic phase in twisted graphitic systems, Nat. Phys. **18**, 196 (2020).

[24] G. Chen, A. L. Sharpe, P. Gallagher, I. T. Rosen, E. J. Fox, L. Jiang, B. Lyu, H. Li, K. Watanabe, T. Taniguchi *et al.*, Signatures of tunable superconductivity in a trilayer graphene moiré superlattice, Nature (London) **572**, 215 (2019).

[25] G. Chen, L. Jiang, S. Wu, B. Lyu, H. Li, B. L. Chittari, K. Watanabe, T. Taniguchi, Z. Shi, J. Jung *et al.*, Evidence of a gate-tunable Mott insulator in a trilayer graphene moiré superlattice, Nat. Phys. **15**, 237 (2019).

[26] H. C. Po, L. Zou, T. Senthil, and A. Vishwanath, Faithful tight-binding models and fragile topology of magic-angle bilayer graphene, Phys. Rev. B **99**, 195455 (2019).

[27] J. Liu, J. Liu, and X. Dai, Pseudo Landau level representation of twisted bilayer graphene: Band topology and implications on the correlated insulating phase, Phys. Rev. B **99**, 155415 (2019).

[28] N. Bultinck, S. Chatterjee, and M. P. Zaletel, Mechanism for Anomalous Hall Ferromagnetism in Twisted Bilayer Graphene, Phys. Rev. Lett. **124**, 166601 (2020).

[29] Z. Song, Z. Wang, W. Shi, G. Li, C. Fang, and B. A. Bernevig, All Magic Angles in Twisted Bilayer Graphene are Topological, Phys. Rev. Lett. **123**, 036401 (2019).

[30] J. Ahn, S. Park, and B.-J. Yang, Failure of Nielsen-Ninomiya Theorem and Fragile Topology in Two-Dimensional Systems with Space-Time Inversion Symmetry: Application to Twisted Bilayer Graphene at Magic Angle, Phys. Rev. X **9**, 021013 (2019).

[31] Y.-H. Zhang, D. Mao, and T. Senthil, Twisted bilayer graphene aligned with hexagonal boron nitride: Anomalous Hall effect and a lattice model, Phys. Rev. Research **1**, 033126 (2019).

[32] J. Liu, Z. Ma, J. Gao, and X. Dai, Quantum Valley Hall Effect, Orbital Magnetism, and Anomalous Hall Effect in Twisted Multilayer Graphene Systems, Phys. Rev. X **9**, 031021 (2019).

[33] R. Bistritzer and A. H. MacDonald, Moiré bands in twisted double-layer graphene, Proc. Natl. Acad. Sci. USA **108**, 12233 (2011).

[34] J. M. B. Lopes dos Santos, N. M. R. Peres, and A. H. Castro Neto, Continuum model of the twisted graphene bilayer, Phys. Rev. B **86**, 155449 (2012).

[35] H. C. Po, L. Zou, A. Vishwanath, and T. Senthil, Origin of Mott Insulating Behavior and Superconductivity in Twisted Bilayer Graphene, Phys. Rev. X **8**, 031089 (2018).

[36] A. Bouhon, A. M. Black-Schaffer, and R.-J. Slager, Wilson loop approach to fragile topology of split elementary band representations and topological crystalline insulators with time-reversal symmetry, Phys. Rev. B **100**, 195135 (2019).

[37] M. Koshino, Band structure and topological properties of twisted double bilayer graphene, Phys. Rev. B **99**, 235406 (2019).

[38] J. Wang and Z. Liu, Hierarchy of Ideal Flatbands in Chiral Twisted Multilayer Graphene Models, Phys. Rev. Lett. **128**, 176403 (2022).

[39] P. J. Ledwith, A. Vishwanath, and E. Khalaf, Family of Ideal Chern Flatbands with Arbitrary Chern Number in Chiral Twisted Graphene Multilayers, Phys. Rev. Lett. **128**, 176404 (2021).

[40] R. D. King-Smith and D. Vanderbilt, Theory of polarization of crystalline solids, Phys. Rev. B **47**, 1651 (1993).

[41] R. Resta and D. Vanderbilt, Theory of polarization: A modern approach, in *Physics of Ferroelectrics: A Modern Perspective*, edited by K. M. Rabe, C. H. Ahn, and J.-M. Triscone (Springer-Verlag, Berlin, 2007).

[42] S. Coh and D. Vanderbilt, Electric Polarization in a Chern Insulator, Phys. Rev. Lett. **102**, 107603 (2009).

[43] D. Vanderbilt, Berry-phase theory of proper piezoelectric response, J. Phys. Chem. Solids **61**, 147 (2000).

[44] H. Suzuura and T. Ando, Phonons and electron-phonon scattering in carbon nanotubes, Phys. Rev. B **65**, 235412 (2002).

[45] V. M. Pereira and A. H. Castro Neto, Strain Engineering of Graphene's Electronic Structure, Phys. Rev. Lett. **103**, 046801 (2009).

[46] N. N. T. Nam and M. Koshino, Lattice relaxation and energy band modulation in twisted bilayer graphene, Phys. Rev. B **96**, 075311 (2017).

[47] Z. Bi, N. F. Q. Yuan, and L. Fu, Designing flat bands by strain, Phys. Rev. B **100**, 035448 (2019).

[48] F. Rost, R. Gupta, M. Fleischmann, D. Weckbecker, N. Ray, J. Olivares, M. Vogl, S. Sharma, O. Pankratov, and S. Shallcross, Nonperturbative theory of effective Hamiltonians for deformations in two-dimensional materials: Moiré systems and dislocations, Phys. Rev. B **100**, 035101 (2019).

[49] J. Yu and C. Liu, Piezoelectricity and topological quantum phase transitions in two-dimensional spin-orbit coupled crystals with time-reversal symmetry, Nat. Commun. **11**, 2290 (2020).

[50] J. M. B. Lopes dos Santos, N. M. R. Peres, and A. H. Castro Neto, Graphene Bilayer with a Twist: Electronic Structure, Phys. Rev. Lett. **99**, 256802 (2007).

[51] D. Weckbecker, S. Shallcross, M. Fleischmann, N. Ray, S. Sharma, and O. Pankratov, Low-energy theory for the graphene twist bilayer, Phys. Rev. B **93**, 035452 (2016).

[52] P. Moon and M. Koshino, Electronic properties of graphene/hexagonal-boron-nitride moiré superlattice, Phys. Rev. B **90**, 155406 (2014).

[53] J. Jung, A. Raoux, Z. Qiao, and A. H. MacDonald, *Ab initio* theory of moiré superlattice bands in layered two-dimensional materials, Phys. Rev. B **89**, 205414 (2014).

[54] See Supplemental Material at http://link.aps.org/supplemental/10.1103/PhysRevResearch.4.L032006 for: (a) the detailed presentation of the continuum models for the twisted bilayer, and twisted multilayer graphene systems; (b) the derivations for the strain induced pseudo vector potentials in graphene; (c) the results of piezoelectric response from atomistic tight-binding calculations; and (d) the piezoelectric response of hBN-aligned TBG in the presence of local strain, heterostrain, and intervalley coupling.

[55] N. N. Klimov, S. Jung, S. Zhu, T. Li, C. A. Wright, S. D. Solares, D. B. Newell, N. B. Zhitenev, and J. A. Stroscio, Electromechanical properties of graphene drumheads, Science **336**, 1557 (2012).

[56] N. Levy, S. A. Burke, K. L. Meaker, M. Panlasigui, A. Zettl, F. Guinea, A. H. C. Neto, and M. F. Crommie, Strain-induced pseudo-magnetic fields greater than 300 tesla in graphene nanobubbles, Science **329**, 544 (2010).

[57] L. Meng, W.-Y. He, H. Zheng, M. Liu, H. Yan, W. Yan, Z.-D. Chu, K. Bai, R.-F. Dou, Y. Zhang, Z. Liu, J.-C. Nie, and L. He, Strain-induced one-dimensional landau level quantization in corrugated graphene, Phys. Rev. B **87**, 205405 (2013).

[58] H. Yan, Y. Sun, L. He, J.-C. Nie, and M. H. W. Chan, Observation of Landau-level-like quantization at 77 k along a

strained-induced graphene ridge, Phys. Rev. B **85**, 035422 (2012).

[59] P. Moon and M. Koshino, Optical absorption in twisted bilayer graphene, Phys. Rev. B **87**, 205404 (2013).

[60] X. He, N. Tang, X. Sun, L. Gan, F. Ke, T. Wang, F. Xu, X. Wang, X. Yang, W. Ge *et al.*, Tuning the graphene work function by uniaxial strain, Appl. Phys. Lett. **106**, 043106 (2015).

[61] R. Gupta, F. Rost, M. Fleischmann, S. Sharma, and S. Shallcross, Straintronics beyond homogeneous deformation, Phys. Rev. B **99**, 125407 (2019).

[62] N. Bultinck, E. Khalaf, S. Liu, S. Chatterjee, A. Vishwanath, and M. P. Zaletel, Ground State and Hidden Symmetry of Magic-Angle Graphene at Even Integer Filling, Phys. Rev. X **10**, 031034 (2020).

[63] Y. Zhang, K. Jiang, Z. Wang, and F. Zhang, Correlated insulating phases of twisted bilayer graphene at commensurate filling fractions: A Hartree-Fock study, Phys. Rev. B **102**, 035136 (2020).

[64] B. Lian, Z.-D. Song, N. Regnault, D. K. Efetov, A. Yazdani, and B. A. Bernevig, Twisted bilayer graphene. IV. Exact insulator ground states and phase diagram, Phys. Rev. B **103**, 205414 (2021).

[65] B. A. Bernevig, Z.-D. Song, N. Regnault, and B. Lian, Twisted bilayer graphene. III. Interacting Hamiltonian and exact symmetries, Phys. Rev. B **103**, 205413 (2021).

[66] Y. H. Kwan, G. Wagner, T. Soejima, M. P. Zaletel, S. H. Simon, S. A. Parameswaran, and N. Bultinck, Kekulé Spiral Order at All Nonzero Integer Fillings in Twisted Bilayer Graphene, Phys. Rev. X **11**, 041063 (2021).

[67] G. Wagner, Y. H. Kwan, N. Bultinck, S. H. Simon, and S. A. Parameswaran, Global Phase Diagram of the Normal State of Twisted Bilayer Graphene, Phys. Rev. Lett. **128**, 156401 (2022).

[68] M. He, Y. Li, J. Cai, Y. Liu, K. Watanabe, T. Taniguchi, X. Xu, and M. Yankowitz, Symmetry breaking in twisted double bilayer graphene, Nat. Phys. **17**, 26 (2021).

[69] J. Xue (private communication).